Nanoscale

ROYAL SOCIETY OF CHEMISTRY

PAPER

View Article Online
View Journal | View Issue

Cite this: *Nanoscale*, 2020, **12**, 6334

Fluorescent dye nano-assemblies by thiol attachment directed to the tips of gold nanorods for effective emission enhancement†

David Botequim, [a,b] Inês I. R. Silva,[a] Sofia G. Serra,[a] Eduardo P. Melo, [c] Duarte M. F. Prazeres, *[b] Sílvia M. B. Costa [a] and Pedro M. R. Paulo *[a]

The conjugation of dye-labelled DNA oligonucleotides with gold nanorods has been widely explored for the development of multifunctional fluorescent nanoprobes. Here, we show that the functionalization route is crucial to achieve enhanced emission in dye nano-assemblies based on gold nanorods. By using a tip-selective approach for thiol attachment of dye molecules onto gold nanorods, it was possible to effectively increase the emission by more than 10-fold relatively to that of a free dye. On the other hand, a non-selective approach revealed that indiscriminate surface functionalization has a detrimental effect on the enhancement. Simulations of discrete dipole approximation gave further insight into the surface distribution of plasmon-enhanced emission by confirming that tip regions afford an effective enhancement, while side regions exhibit a negligible effect or even emission quenching. The contrast between dye nano-assemblies obtained from tip- and non-selective functionalization was further characterized by single-particle fluorescence emission. These studies showed that tip-functionalized gold nanorods with an average of only 30 dye molecules have a comparable to or even stronger emission than non-selectively functionalized particles with approximately 10 times more dye molecules. The results herein reported could significantly improve the performance of dye nano-assemblies for imaging or sensing applications.

Received 9th January 2020,
Accepted 22nd February 2020

DOI: 10.1039/d0nr00267d

rsc.li/nanoscale

1. Introduction

The assembly of nano-objects composed of fluorescent dyes, or other emitters, and metal nanoparticles is a promising approach for the development of multifunctional probes that can be addressed by optical techniques in biological systems to perform imaging, sensing, drug delivery or other therapeutic functions.[1,2] In these nano-assemblies, the role of metal nanoparticles is frequently more than just that of a nano-sized carrier owing to their extraordinary optical properties, and in particular, their ability to perform as optical antennas for fluorescent dyes.[3] Gold nanorods have been extensively investigated for this purpose due to their many advantages, namely, the chemical stability of gold combined with well-established colloidal methods for nanorod synthesis with controlled size and shape dispersion, the ability to tune their optical response across the near-infrared biological window by changing their aspect ratio, and the large plasmon near-field at the nanorod tips provided by the longitudinal surface plasmon mode.[4]

Early reports on dye nano-assemblies based on gold nanorods were mostly concerned on the fundamental properties of plasmon-coupled emission such as fluorescence enhancement,[5–8] emission directionality,[6,9] spectral reshap-

[a]*Centro de Química Estrutural, Instituto Superior Técnico, Universidade de Lisboa, Av. Rovisco Pais 1, 1049-001 Lisboa, Portugal.*
E-mail: pedro.m.paulo@tecnico.ulisboa.pt
[b]*iBB-Institute for Bioengineering and Biosciences, Instituto Superior Técnico, Universidade de Lisboa, Av. Rovisco Pais 1, 1049-001 Lisboa, Portugal.*
E-mail: miguelprazeres@tecnico.ulisboa.pt
[c]*CCMAR - Centro de Ciências do Mar, Universidade do Algarve, Campus de Gambelas, 8005-139 Faro, Portugal*

†Electronic supplementary information (ESI) available: Additional fluorescence enhancement factors from DDA simulations. Emission spectra of dye displaced from dye-particle nano-assemblies. Normalized emission spectra of tip-functionalized gold nanorods. Emission spectra of the "NS-4000" sample for several excitation wavelengths. Spectral dependence of the calculated enhancement factors from DDA simulations. Analysis of autocorrelation function curves from single-particle fluorescence emission. Examples of intensity time traces of two control systems measured by confocal fluorescence microscopy. Fluorescence decays of dye-particle nano-assemblies in colloidal suspension. Cell internalization assays. Comparison with literature examples. Working curve for the determination of dye-labelled oligonucleotide concentration. Evaluation of fluorescence enhancement in tip-functionalized gold nanorods. Zeta potential of dye-particle nano-assemblies in aqueous suspension. Validation of tip-selective functionalization. Evaluation of photobleaching effects. See DOI: 10.1039/d0nr00267d

ing,[10] or assisted energy transfer processes.[11] More recently, there have been numerous reports on dye-nanorod assemblies as dual mode probes for combined imaging and therapeutic functions, such as photothermal or photodynamic therapy,[12–25] or for sensing intracellular components.[26–31] In this view, gold nanorods have been conjugated with a diversity of organic dyes, such as cyanines,[13,16,22] phthalocyanines,[12,24] porphyrins[21,25,28] and chlorins,[15,23] and also with inorganic emitters, such as semiconductor quantum-dots,[18,26] rare-earth doped particles[32] and metal clusters.[27] The strategies of dye-particle assembly also comprise a diversity of approaches such as chemical attachment of dye molecules using thiol derivatization,[15,16] non-covalent supramolecular assembly,[19,21] entrapment in a polymer or silica shell,[12,14] or even a combination of the previous strategies.[13,18] In most of these examples, the overall emission of the nano-assemblies is less than, or at most comparable to, that of the same amount of fluorescent dye loaded onto the nanoparticle.[12,18] Therefore, the plasmonic antenna effect of gold nanorods is not being explored for enhancing the bioimaging functionality in these systems. In fact, there are only a limited number of reports in which an effective fluorescence enhancement is clearly demonstrated.[24,25,28] Furthermore, in these nano-assemblies, the dye molecules are indiscriminately attached over the whole surface of the gold nanorods, instead of being concentrated at the tips, where plasmon hot-spots for emission enhancement are located.[4]

The colloidal stabilization of gold nanorods by a cetyltrimethylammonium bromide (CTAB) surfactant bilayer offers a straightforward approach for tip-specific functionalization using thiol-derivatized molecules. The role of CTAB detergent as a side-protective reagent that directs thiol attachment toward the nanorod tips has long been reported in the literature and explored for controlled end-to-end nanorod assembly.[33–35] Later, it was also explored for selectively attaching dye molecules mediated by biotin–streptavidin binding onto the tips of gold nanorods, which yielded enhancements of about 40-fold from single-molecule fluorescence emission.[36] The ability of gold nanorods to perform as optical antennas that afford large fluorescence enhancements has been demonstrated for a diversity of emitters using single-molecule fluorescence detection.[37–39] In particular, it was shown that for weakly fluorescent molecules the overall enhancement factors can surpass a 1000-fold emission increase for resonant plasmonic enhancement of fluorescence.[37] On the other hand, the large enhancement factors observed for dye-particle systems that are prepared, or selected, in single-molecule experiments may be difficult to achieve under ensemble conditions. The enhancement factors are more modest for dye-nanorod assemblies, typically in the range of 10-fold emission increase, due to sample averaging over many dye molecules positioned randomly, instead of being concentrated at the plasmon hot-spots.[5–8] In this view, the optimization of dye-particle attachment in such nano-assemblies is critical to maximize the enhancement effect of the gold nanorod antenna.

In this work, we have compared two functionalization strategies to prepare dye-particle nano-assemblies using thiol attachment of dye-labelled dsDNA oligonucleotides onto gold nanorods. The nano-assemblies were prepared either by a tip-specific approach using a CTAB side-protective bilayer, or by a non-selective approach, that consists of a two-step ligand exchange process. The emission properties of these dye-particle nano-assemblies were investigated by ensemble spectroscopy and single-particle fluorescence microscopy. Briefly, it was found that only tip-specific functionalization afforded an effective fluorescence enhancement effect of more than 10-fold increase in the emission, which confirms that site-selective functionalization strategies are important to maximize antenna effects.

2. Results and discussion

The modification of gold nanoparticles with thiolated oligonucleotides has enabled the use of DNA-directed assembly to achieve precise positioning of particles or molecular components in the development of nano-composite materials. In this work, we were interested in exploring DNA linkers as a spacer between the metal surface of a gold nanorod and a fluorescent dye, in order to develop dye-particle nano-assemblies with enhanced emission properties. The double-stranded DNA linker used is assembled by combining two complementary 10-nt sequences that are terminated with thiol groups. The opposite side of one of the oligonucleotides is labelled with one Atto-647N dye molecule (Fig. 1). The length of this sequence, which is *ca.* 3.4 nm, was chosen to approximately match the optimal distance for emission enhancement at the nanorod tips, as estimated from model simulations using the Discrete Dipole Approximation (DDA) method (Fig. S1 of the ESI†). Our initial aim was to maximize the thiol attachment at the nanorod tips which would concentrate dye molecules in the hot-spot regions. As previously mentioned, the colloidal stabilization of gold nanorods by a CTAB bilayer has been widely employed for achieving tip-selective functionalization of these particles with thiolated molecules.[33–36,40,41] However, in the case of DNA oligonucleotides, which are strongly negatively charged, their attachment onto CTAB-stabilized gold particles may be facilitated by the addition of salt and/or co-surfactants, such as SDS, Tween or PVP. In some examples, this process is carried out in two steps so that CTAB is first completely replaced by another surface agent before binding of the thiolated oligonucleotides.[42,43] Even though this approach allows for a better control over particle stability, it usually implies the loss of the CTAB side-protective role that directs the tip attachment of thiols and, thus, it results in the functionalization of the particle surface in a non-selective fashion. We have chosen to compare two approaches for the functionalization of gold nanorods with thiolated oligonucleotides: a non-selective coating *via* a two-step ligand exchange, hereafter termed "NS" functionalization, and a tip-selective approach using the CTAB as a directing reagent through its side protective role, hereafter

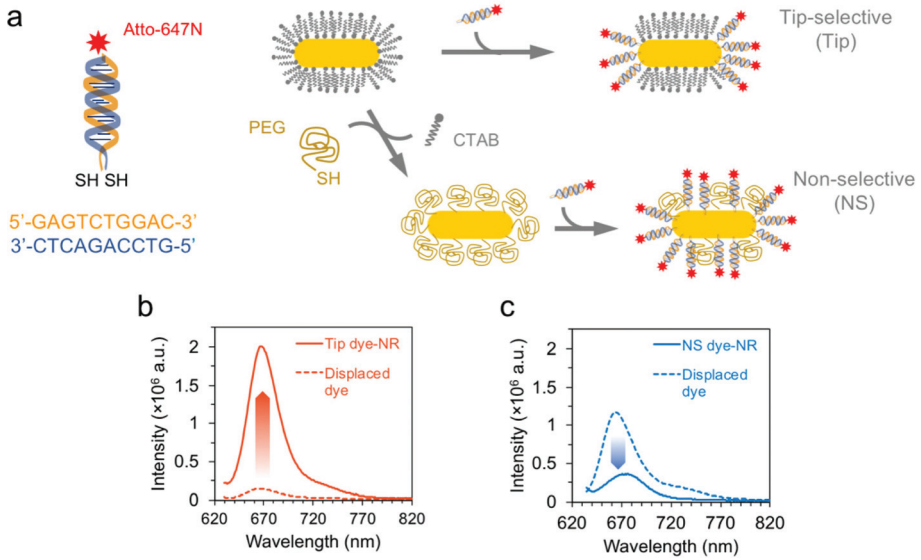

Fig. 1 (a) Scheme of a dye-labelled dsDNA oligonucleotide and preparation of dye-particle nano-assemblies using two functionalization methods: (top) tip-selective or "Tip" is based on the protective role of the side walls of the CTAB bilayer in direct thiol attachment toward the nanorod tips; (bottom) non-selective or "NS" is a two-step coating process in which CTAB is first replaced with thiolated PEG and then fluorescently-labelled DNA oligonucleotides are inserted; (b) emission spectra of tip-functionalized nano-assemblies (solid line) and of the dye-labelled oligonucleotides from the same sample displaced into solution by ligand exchange with 2-mercaptoethanol (dashed line); (c) emission spectra of NS-functionalized nano-assemblies (solid line) and of its displaced dye-labelled oligonucleotides (dashed line). Excitation wavelength was 620 nm in both parts (b) and (c).

termed "tip" functionalization (Fig. 1a). The comparison between these two approaches provided a demonstration of the critical role of surface chemistry in the outcome properties of these systems – both resulted in strongly emitting dye-particle nano-assemblies, but only tip-functionalization showed evidence of an effective antenna effect, in which the emission from the assembly is larger than its isolated components.

2.1 Fluorescence enhancement in tip-functionalized assemblies

The fluorescence enhancement effect was experimentally assessed by comparing the emission spectrum from a sample of dye-particle nano-assemblies with that from the same sample after displacing the dye molecules into solution by ligand exchange with 2-mercaptoethanol.[44] For tip-functionalized samples, this method consistently afforded larger emission intensities for dye-particle nano-assemblies than that for displaced dye molecules, thus, showing an effective emission enhancement (Fig. 1b). On the other hand, the dye-particle nano-assemblies obtained by NS-functionalization often show more emission from its displaced dye into solution, which means that overall the dye's emission is suppressed in these nano-assemblies (Fig. 1c).

We have further investigated this subject by evaluating how the amount of dye loaded per particle affects the fluorescence enhancement in tip-functionalized nano-assemblies (Fig. 2). The emission intensity of displaced dye increases proportionally to the incubation time during their functionalization, which indicates that larger amounts of dye are being loaded onto the nanorods (Fig. S2 in the ESI†). The dye-per-particle ratio corresponds on average to approximately 36, 53 and 93 dye molecules for incubation times of 1, 3 and 6 hours, respectively (Fig. 2c). These values are well below the theoretical maximum of 412 oligos estimated from the empirical footprint of a short ssDNA chain, as proposed in ref. 45, and are also below those determined experimentally by other authors for fully coated gold nanorods of similar size.[46,47] Thus, it is reasonable to assume that the surface of gold nanorods is not saturated even for an incubation time of 6 hours. However, as more dye is added by extending the incubation time, it is also likely that insertion at the nanorod side becomes more relevant. As discussed further ahead (section 2.3), the loading of dye molecules on the particle side should have a negative contribution to the average emission enhancement, as these surface regions provide little or no enhancement effect. Indeed, the largest enhancement factor was evaluated for an incubation of 1 hour and the trend shows a gradual decrease of enhancement factors as incubation time increases (Fig. 2d). The apparent effect of emission saturation is tentatively explained if the tip surface becomes saturated already at the lowest dye-per-particle ratio and the dye molecules that are further loaded by increasing dye-per-particle ratio become inserted in the side regions, thus giving a negligible contribution to the overall dye-particle emission.

The extinction spectrum of tip-functionalized nano-assemblies compared to that of the original CTAB-stabilized gold nanorods shows that the plasmon peak wavelength is red-shifted by about 10 nanometres (inset of Fig. 2a) and, also the spectral lineshape broadens. These effects may result from a combination of factors. First, the replacement of CTAB surfac-

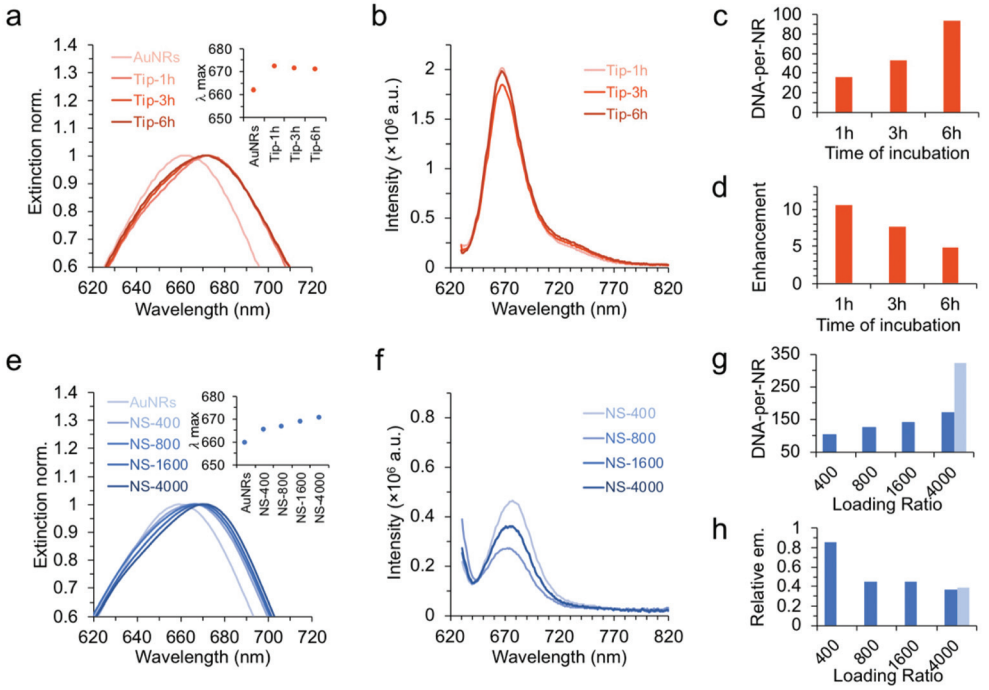

Fig. 2 Evaluation of fluorescence enhancement in dye-particle nano-assemblies: (a, b) extinction and emission spectra of tip-selective functionalized gold nanorod samples for several incubation times – the inset in part (a) shows the extinction peak wavelength (λ_{max}); (c) number of dye-labelled DNA chains per nanorod ("DNA-per-NR"); (d) experimental fluorescence enhancement factor of tip-functionalized gold nanorods determined for excitation at 620 nm; (e, f) extinction and emission spectra of non-selective functionalized gold nanorod samples for various DNA loading ratios – the inset in part (e) shows the extinction peak wavelength (λ_{max}); (g) number of dye-labelled DNA chains per nanorod ("DNA-per-NR"); (h) experimental relative emission showing quenching in non-selective functionalized gold nanorods determined for excitation at 620 nm. The light blue bars in parts (g) and (h) refer to a non-selective functionalization sample prepared with an overnight incubation time.

tant molecules by DNA oligonucleotide chains is likely to contribute to a change of local refraction index in the tip regions, which could account for the peak shift of the surface plasmon resonance, while particle-to-particle variability in the number of attached DNA chains may contribute as a source of inhomogeneous line broadening. Second, the dye-particle extinction also includes a contribution from the plasmon-enhanced absorption of light by its coupled dye molecules. It is not straightforward to separate the above-mentioned two effects on the overall extinction spectrum, in order to experimentally assess only the enhancement factor on the dye's absorption.

2.2 Excitation wavelength dependence of the enhancement

We have also investigated the dependence of emission enhancement on the excitation wavelength. It could be anticipated that emission enhancement increases as the excitation wavelength is brought closer to the longitudinal surface plasmon resonance, because the induced plasmon near-field becomes stronger, thus, producing larger accelerations in the dye's excitation rate. We have explored this feature by selecting excitation wavelengths on the high energy side of the longitudinal surface plasmon band until the dye's Stokes shift allowed the measurement of the maximum emission peak, as illustrated here for tip-functionalized nano-assemblies with an incubation time of 1 hour (Fig. 3). It was possible to confirm that the emission enhancement increases from a factor of about 7 up to 17-fold when the excitation wavelength varies from 600 to 650 nm, as it approaches the longitudinal surface plasmon peak of these gold nanorods. In the samples prepared with incubation times of 3 and 6 hours, we have observed the same trend, although the enhancement factors are smaller in magnitude, as previously discussed. The dependence of the enhancement factor on the excitation wavelength, as shown here, qualitatively supports the role of plasmon-enhanced fluorescence in the emission from these dye-particle nano-assemblies. Intriguingly, no significant changes were observed in the lineshape of the enhanced emission spectra, as inferred from a comparison between the normalized emission from dye-particle nano-assemblies and that of the displaced dye molecules (inset of Fig. 3a and Fig. S3 of the ESI†). The apparent absence of spectral reshaping in the plasmon-coupled emission of our dye-particle assemblies may result from a good spectral overlap between the dye's emission and the longitudinal surface plasmon band, as suggested from the simulated spectra shown in Fig. S3b and c of the ESI.†

The samples prepared by NS-functionalization can also be tuned in terms of the amount of dye-labelled DNA attached per particle (Fig. 2e and f). By keeping the incubation time fixed at 1 hour, it was possible to gradually increase the number of DNA chains attached per particle from about 102 up to 170 by successively increasing the loading ratio from 400 to 4000 during incubation (Fig. 2g). In the latter case, it was

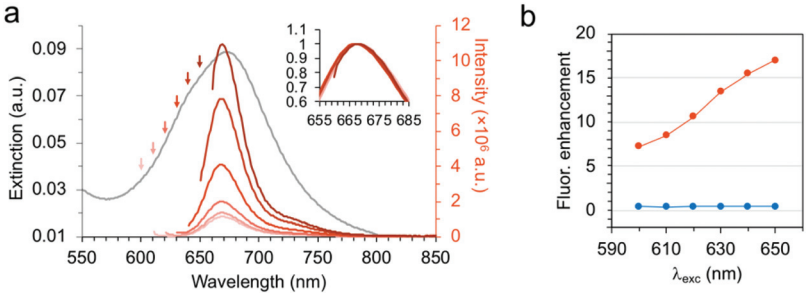

Fig. 3 Evaluation of fluorescence enhancement of tip-functionalized gold nanorods and its dependence on the excitation wavelength: (a) extinction spectrum of dye-particle nano-assemblies for the "Tip-1h" sample (grey curve) and emission spectra of the same sample for several excitation wavelengths (red curves) indicated by the arrows over the extinction spectrum – the inset is an overlay of the normalized emission spectra showing that the lineshape practically does not change; (b) experimental fluorescence enhancement factor of dye-particle nano-assemblies for the "Tip-1h" sample (red symbols) and comparison with non-selectively functionalized gold nanorods for the "NS-4000" sample (blue symbols).

further possible to almost double the number of the attached chains up to 327 by extending the incubation time from 1 hour to overnight (light blue-coloured bar). However, the emission intensity from NS-functionalized samples is at most comparable to that of the displaced dye into solution, and more frequently than not, it is actually less intense (Fig. 2f and S2b in the ESI†). So, the average emission from dye molecules in the nano-assemblies prepared by NS-functionalization is suppressed (Fig. 2h). The absence of an effective emission enhancement, or antenna effect, in these ensemble measurements does not mean that the dye-particle nano-assemblies are not strongly emissive as individual objects, a fact that was confirmed by fluorescence microscopy (section 2.5). The non-selective functionalization seems to produce nano-assemblies in which there is a compensation between the antenna effect known for dye molecules positioned at the rod tips and quenching processes that may result from the predominance of non-radiative decay enhancement at the particle sides or from self-quenching interactions due to close packing of dye molecules on the particle surface. A comparison of the antenna effect on the dye's emission between the tip and side positions at the nanorod surface was examined by model simulations, as detailed below. Moreover, the spectral dependence on the excitation wavelength in these dye-particle nano-assemblies shows a distinct behaviour relatively to tip-functionalized samples that was tentatively attributed to molecular aggregation. In particular, the emission peak maximum displays a significant blue-shift as excitation is selected at longer wavelengths (Fig. S4 of the ESI†). Also, the lineshape of these spectra differs from that of the displaced dye in solution by presenting a lower relative intensity of the second vibronic. These characteristics are amenable for an excitonic interaction of H-type, as known for molecular dye aggregates in which π-stacking of conjugated macrocyclic dyes results in a colinear alignment of their transition dipoles.[48] The lowest excitonic state of H-aggregates is usually a dark state because of cancellation between the individual transition dipoles of the coupled molecules, which could explain the absence of emission enhancement in the NS-functionalized samples. However, this excitonic interaction would have to be in the weak coupling regime due to the absence of major spectral changes. Alternative explanations for the spectral wavelength dependence could invoke a solvatochromic type of shift in the local environment at the nanorod surface and the spectral selection of a sub-population of dye molecules upon changing the excitation wavelength.

2.3 Model simulations of a single dye on a gold nanorod

The contrast between the emission properties of nano-assemblies prepared by tip- and NS-functionalization illustrates the importance of site-selective approaches for particle conjugation with functional molecular components. Site-selective approaches enable the concentration of the desired functionality at the plasmon hot-spots, thus, maximizing the intended effects in the nano-composite systems, either for enhancing fluorescence emission by antenna effects, or for molecular sensing based on the refraction index sensitivity of the plasmon resonance. The spatial heterogeneity of plasmon-molecule interactions has motivated us to perform detailed model simulations of the antenna effect for different dye positions on the particle surface (Fig. 4). Our aim was to clearly show the differences of emission enhancement between the tip and side regions of the nanorod geometry. For this purpose, the excitation rate enhancement (E_{exc}) and the radiative (K_r) and non-radiative (K_{nr}) decay rates of an emitter were estimated for selected positions on the particle surface in the tip and side regions. Along with the intrinsic radiative (k_0) and non-radiative (k_{nr}) decay rates of Atto-647N in water, it was possible to estimate a fluorescence enhancement factor ($F/F^0|_{calc}$) for each emitter position, as indicated in Fig. 4a.

Simulations were performed within a wavelength interval covering the absorption and emission spectra of Atto-647N dye, in order to retrieve spectrally averaged enhancement factors that could afford a fair comparison with the experimental ones. The plots of Fig. 4b–d provide detailed insight into the spectral dependence of the enhancement effect on each photophysical rate, which has been previously discussed.[37] Furthermore, it also illustrates the enhancement dependence on the dye's orientation relative to the nanorod particle. Fig. 4e shows the complete set of emitter positions

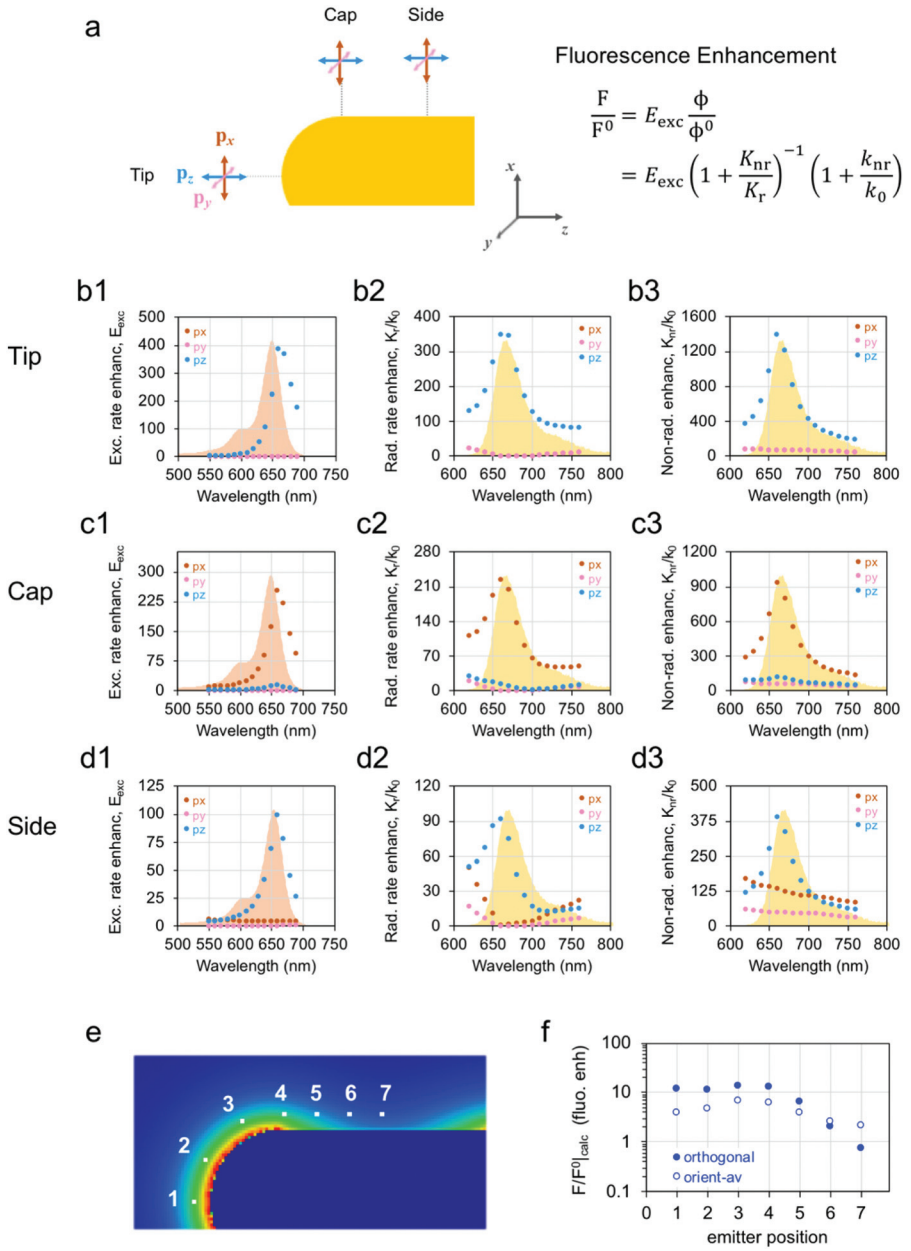

Fig. 4 Theoretical estimation of fluorescence enhancement using DDA simulations: (a) scheme of the dye-particle model showing the dye emitter in three selected positions of tip, cap and side – the enhancement factor is calculated from $F/F^0|_{calc} = E_{exc} \times \phi/\phi^0$ using the excitation rate enhancement and the relative fluorescence quantum yield (see the Experimental section for other details); (b–d) enhancement factors for the excitation, radiative and non-radiative decay rates (E_{exc}, K_r and K_{nr}, respectively) of an emitter in the tip, cap and side regions – for comparison, the normalized absorption or emission spectrum of Atto-647N dye is shown in the background (orange and yellow shaded areas, respectively), also, the decay rates were normalized by the dye's intrinsic radiative decay rate ($k_0 = 1.4 \times 10^8$ s^{-1}); (e) set of emitter positions considered on the particle surface displayed on the near-field enhancement map of the simulated gold nanorod for excitation at 620 nm; (f) fluorescence enhancement factors calculated from DDA simulations for different emitter positions considering either an orthogonal orientation of the emitter's dipole (closed symbols) or an average orientation (open symbols).

probed on the particle surface superimposed on the near-field enhancement map calculated for excitation at 620 nm. This wavelength was chosen to coincide with the data shown in Fig. 2b and d. The enhancement factors displayed in Fig. 4f show that these do not vary significantly in the tip region (positions 1–4) and correspond to an emission increase of about 10-fold (or slightly smaller, if orientation averaging of the emitter's dipole is considered). The emission enhancement decreases away from the tip region (position 4) when proceeding towards the rod side (position 7). Accordingly, in the middle position the dye's emission should be suppressed for an orthogonal orientation of the emitter's dipole. The

simulation results confirm that the dispersion of dye molecules over the side regions of a gold nanorod antenna should, on the overall, contribute to a lower emission enhancement effect. The difference between the tip and side regions increases steeply as the excitation wavelength comes closer to the surface plasmon resonance peak (Fig. S5 in the ESI†), showing that the distribution of dye attachment affects more critically the overall enhancement in that condition. A direct quantitative comparison between simulations and experimental results may be impaired by sample's heterogeneity in the distribution of particle size and shape and also by variations from particle-to-particle in the number of dye molecules attached. Nevertheless, the simulations show that distributing dye molecules non-selectively over the surface will decrease the overall antenna effect as opposed to concentrating the same (or a smaller) amount of dye at the plasmon hot-spots in the tip regions.

2.4 Single-particle emission in colloidal suspension

The emission properties of the dye-particle nano-assemblies were further investigated at the single-particle detection level by confocal fluorescence microscopy. The emission intensity time traces from dilute colloidal suspensions of these nano-assemblies with sub-nanomolar concentrations show intense fluorescence burst events with maximum photon detection rates in the order of hundreds of counts per ms for an excitation power of only 4.4×10^{-3} kW cm^{-2} (Fig. 5). Further information from these intensity traces was obtained from their autocorrelation function (ACF), as shown in Fig. 5e and f. The ACF curves show two relaxation components that were attributed to the rotational and translational diffusion motions of the dye-particle nano-assemblies in colloidal suspension.[49]

The relaxation times fitted for the short and long relaxation times ($\tau_\perp$ an τ_w) correspond to the values theoretically estimated using a modified version of Einstein–Smoluchowski relation for a rod-like particle geometry (Table S1 of the ESI†).[50]

The analysis of ACF curves also provided an estimate of the average occupation number $\langle N \rangle$ of dye-labelled particles in the confocal volume, which was combined with the mean trace intensity $\langle I \rangle$ to determine individual brightness $\langle I \rangle / \langle N \rangle$, which is a sample average for single-particle emission. The comparison between the values of $\langle I \rangle / \langle N \rangle$ shows that tip-functionalized nano-assemblies are stronger emitters than the NS-functionalized ones and that, in general, dye-particle nano-assemblies have an emission that is approximately three orders of magnitude more intense than that of a single dye-labelled oligonucleotide (Fig. 5g). The photoluminescence emission from the gold nanorods alone (without dye) that can be directly excited by one-photon absorption is also negligible (orange triangles), when compared with the emission from dye-particle nano-assemblies. The qualitative trends observed in the individual brightness of tip- and NS-functionalized nano-assemblies are consistent with the results from ensemble emission. The fluorescence decays of dye-particle nano-assemblies show ultrafast decays that are below the setup's time resolution (Fig. S7 of the ESI†).

2.5 Single-particle fluorescence imaging

The chemical attachment of dye molecules onto colloidal nanoparticles is a stochastic process that is prone to originate a dispersion of the number of dye molecules attached per particle.[51–53] The heterogeneity in the degree of dye-labelling will affect the individual brightness of dye-particle nano-assemblies, and thus it will have crucial implications on their performance as single-object nano-probes. In order to characterize the variation of emission properties from particle to particle and between differently functionalized samples, we have performed single-particle fluorescence measurements on surface-immobilized dye-particle assemblies. In these measurements, the excitation laser beam is not polarized on the sample's plane, which means that immobilized objects have approximately the same probability of being excited independently of their orientation on the surface. Nevertheless, it was clearly perceptible that the emission intensity from the diffraction-limited spots in the sampled images showed a certain degree of particle-to-particle variability (Fig. 6). The maximum emission intensity was obtained from point-spread function (PSF) fitting and the single-particle photoluminescence spectrum of each nano-object was obtained in order to confirm that a single gold nanorod was being measured (Fig. 6b and c).

We have selected four samples of dye-particle nano-assemblies in order to compare the emission properties of tip- and NS-functionalization. Firstly, tip-functionalized particles with 1 hour incubation ("Tip-1h") are compared with non-selectively functionalized particles with a dye-per-particle loading ratio of 4000 and incubated overnight ("NS-4000"). This pair of samples affords a comparison between the dye-particle nano-assemblies of the lowest and highest dye content, respectively, of 36 and 327 dye molecules per particle for "Tip-1h" and "NS-4000" samples (Fig. 2c and g). In the second comparison, the tip-functionalized particles for 6 hours ("Tip-6h") are compared with the non-selective functionalized particles incubated with a dye-per-particle ratio of 400 ("NS-400"). This pair of samples affords a comparison between the dye-particle nano-assemblies with approximately the same dye content of 93 and 102 dye molecules per particle, respectively for "Tip-6h" and "NS-400", but prepared with a different functionalization protocol.

The emission intensities of individual particles in samples "Tip-1h" and "NS-4000" are distributed in a similar way, despite their striking difference in the average number of dye molecules per particle (Fig. 6d and f). Remarkably, the "Tip-1h" sample with an average of only 36 dye molecules per particle is composed of objects with an emission intensity comparable to those in "NS-4000" that have an average dye content *ca.* 10 times larger. It is plausible to assume that the emission properties of tip-functionalized samples are dominated by dye molecules attached to the tip hot-spots, which will produce the largest antenna effects. The non-selective functionalization

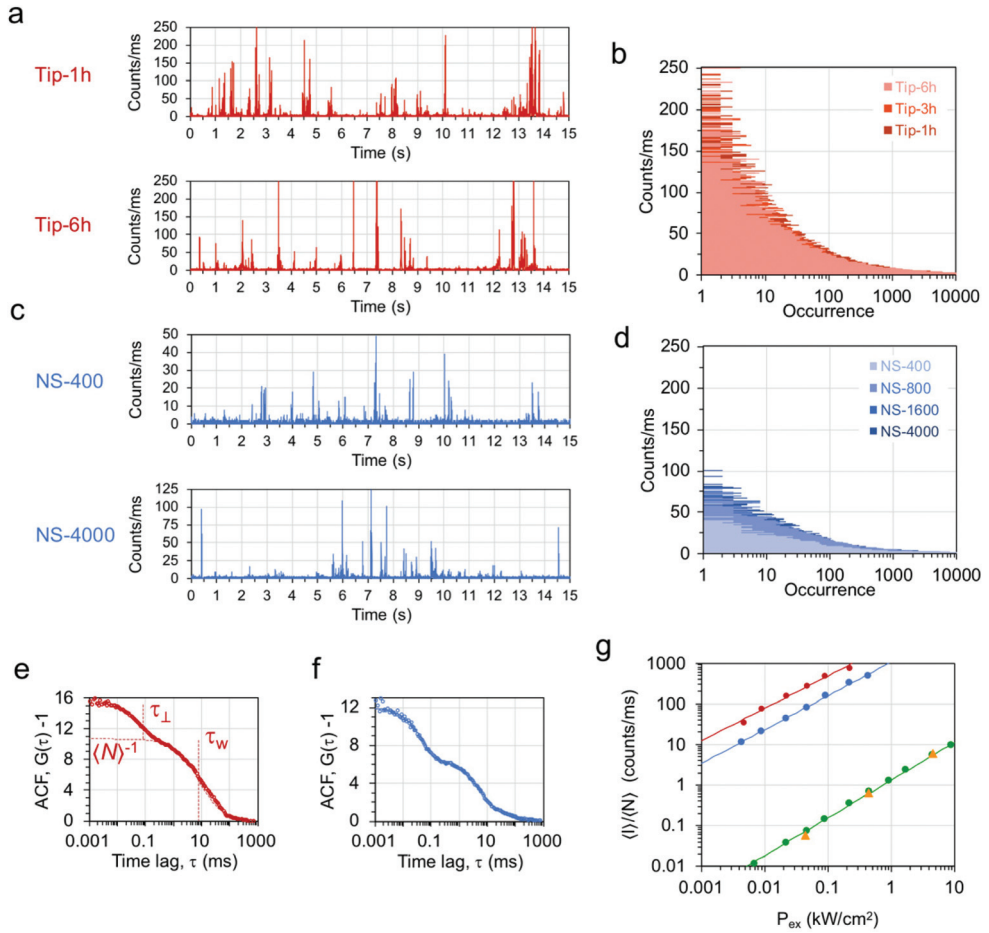

Fig. 5 Fluorescence emission of dye-particle nano-assemblies characterized by confocal fluorescence microscopy: (a) intensity time traces and (b) photon counting histograms of sub-nanomolar suspensions of tip-functionalized gold nanorod samples obtained for excitation at 639 nm with a power of 4.4 $\times 10^{-3}$ kW cm^{-2} – traces are shown for a binning interval of 1 ms; (c, d) similar plots for NS-functionalized gold nanorod samples; (e, f) fluorescence autocorrelation function (ACF) of dye-particle nano-assemblies obtained by tip- and NS-functionalization, respectively; (g) values of individual brightness $\langle I \rangle / \langle N \rangle$ obtained from intensity traces, as a function of the excitation power (P_{ex}) for tip-functionalized samples (red symbols) and for non-selectively functionalized samples (blue symbols) – for comparison, the individual brightness of a single dye-labeled DNA chain (green symbols) and that from one-photon luminescence emission of single gold nanorods (orange triangles) is shown.

with high loading ratios of dye molecules, such as sample "NS-4000", will also have a significant number of dye molecules attached at the tips. This comparison is only effective for non-selective functionalization at high dye contents, because otherwise the dispersion of dye molecules over the surface regions of weak enhancement will negatively affect the individual brightness of dye-particle assemblies. For instance, the "NS-400" sample is mostly composed of objects with less than 100 counts of peak intensity. This sample can be compared with "Tip-6h", which has a similar average number of dye molecules per particle, but displays a distribution of stronger emission intensities (Fig. 6e and g). The differences between tip- and non-selective functionalization may also be appreciated in the spectral properties of individual nano-objects. For instance, the plasmon peak wavelength of surface-immobilized samples is strongly red-shifted in non-selectively functionalized dye-particles relatively to tip-functionalized dye-particles. This result is consistent with the formation of a thicker organic coating layer around dye-particles prepared by non-selective functionalization, because of the combination of attached PEG and DNA chains onto the gold nanorod surface.

The conjugation of gold nanoparticles with DNA oligonucleotides opens up the possibility of developing multi-functional nano-composite systems that combine the strong optical response of plasmonic nanoparticles with the molecular recognition capability of DNA biotechnology, such as molecular beacons or aptamers. These nano-assemblies are particularly promising for *in situ* probing of biological processes in live cells, or *in vivo* conditions, using fluorescence imaging. In order to confirm the potential of the dye-particle nano-assemblies developed here for future applications in live cell studies, we have investigated cell internalization by confocal fluorescence microscopy with sub-diffraction spatial resolution. The "NS-4000" sample was chosen because it is already biocompatible after preparation by ligand exchange of CTAB with a PEG coating. For internalization assays, mouse neuroblas-

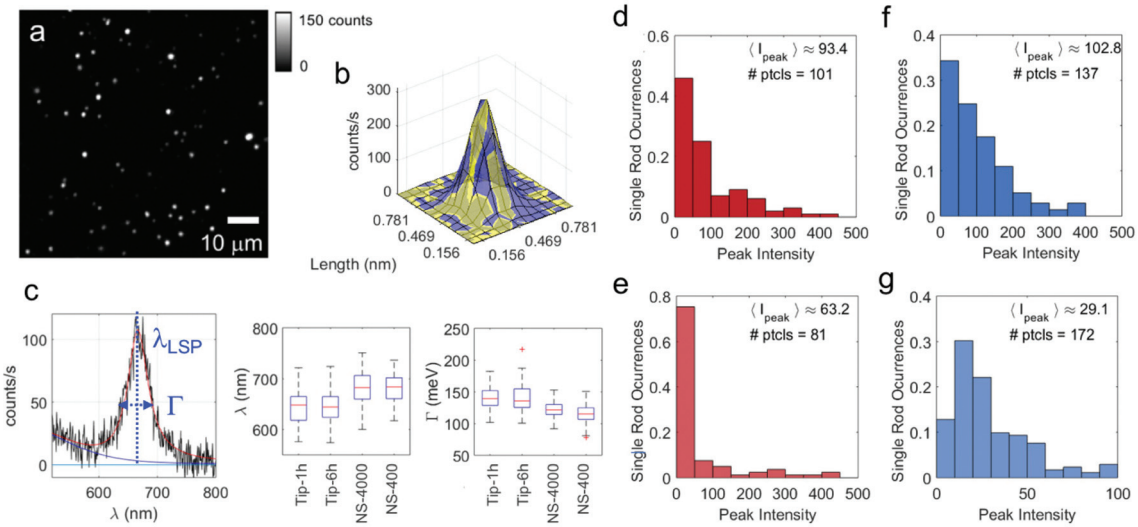

Fig. 6 (a) Fluorescence image of a tip-functionalized sample of dye-particle nano-assemblies dispersed on a PVA polymer film – excitation at 639 nm; (b) example of PSF fitting used to determine the emission intensity ("Peak intensity") of individual nano-assemblies (experimental – yellow surface, and fitted 2D-Gaussian – blue surface); (c) example of the photoluminescence spectrum from a single-particle and of a Lorentzian fitting used to determine the peak wavelength (λ_{LSP}) and linewidth (Γ) – the fitted parameters are shown as box plots in the right panels; (d, e) histograms of the emission peak intensity sampled for individual nano-assemblies of tip-functionalized samples, "Tip-1h" and "Tip-6h", respectively; (f, g) histograms of the emission peak intensity for NS-functionalized samples, "NS-4000" (incubated overnight) and "NS-400", respectively – the insets show the sample average emission intensity, I_{peak}, and the total number of particles sampled.

toma N2a cells were used, which have been genetically modified to express a fusion construct of prion protein with yellow fluorescent protein anchored to the plasma membrane for fluorescence labelling of the cell contour.[54] Live N2a cells were incubated in the presence of a sub-nanomolar concentration of fluorescent particles from the "NS-4000" sample that corresponded to a density of 24 particles per μm^2. After one day of incubation time, it was already possible to verify the uptake of these fluorescent particles by the N2a cells (Fig. S8 in the ESI†). Fig. S8c† shows that red-emitting fluorescent dye-particles have been internalized by the cells and, from the orthogonal projection, it is clear that these particles are present inside the cells. The internalization of dye-particle nano-assemblies and their successful detection inside living cells will be further exploited for developing nano-assemblies carrying functional DNA constructs for nucleic acid sensing, which could have potential for probing gene transcription inside living cells. These studies will be focused on tip-functionalized gold nanorods, because an effective emission enhancement is observed with a low number of attached dye molecules, which leaves more surface available for loading other cargo or functional units onto these nano-assemblies. The use of tip-selective approaches for the assembly of fluorescent probes based on gold nanorods is not commonly explored in most literature reports, which means that those systems may suffer from poor enhancement of dye molecules positioned at the nanorods' side. The comparison between enhancement factors previously reported could serve as a benchmark for evaluating the advantages of tip- over non-selective functionalization. Such a comparison is provided in Table S2 of the ESI.† However, instead of a direct comparison between enhancement factors, which may depend critically on the selected dye's intrinsic quantum yield, it is more relevant to use a figure-of-merit proposed in the literature.[55] This is mostly pertinent for the dye-particle assemblies developed in this work, because Atto-647N dye has already a high quantum-yield of *ca.* 65% in aqueous medium. The figure-of-merit evaluated for the several examples presented in Table S2† shows that tip-selective functionalization, as proposed here, stands out in terms of the achieved enhancement effect.

3. Conclusions

We have shown that the functionalization route for conjugation of dye-labelled DNA oligonucleotides onto gold nanoparticles is crucial for achieving effective plasmon-enhanced emission from these nano-assemblies. By using a procedure for thiol attachment directed to the nanorod tips where plasmon hot-spots are located, it was possible to measure an ensemble effect of emission enhancement of about one order of magnitude in tip-functionalized nano-assemblies. On the other hand, the comparison with a non-selective coating procedure showed that attaching dye molecules indiscriminately over the surface is detrimental for observing emission enhancement. In fact, our results show that, in order to obtain dye-particle nano-assemblies displaying comparable fluorescence emission, the non-selective approach requires a much larger number of dye molecules loaded per particle than the tip-functionalization approach.

4. Experimental

4.1 Materials

Gold nanorods in aqueous suspension stabilized by CTAB with an average size of 25 nm × 71 nm were purchased from Nanopartz Inc. (Loveland, USA) – product no. A12-25-650-CTAB-DIH-25, lot F3216. DNA oligonucleotides purified by HPLC were purchased from STAB Vida (Monte da Caparica, Portugal) with the following sequences: a dye-labeled strand, (Atto-647N)-5′-GAGTCTGGAC-(C6-SH)-3′ and a non-labelled complementary strand, 3′-CTCAGACCTG-(C6-SH)-5′, where C6 stands for a hexamethylene spacer. Thiolated poly(ethylene glycol) (mPEG-SH, MW~5000), Tween 20, CTAB (≥99%) and poly(vinyl alcohol) (PVA, 99%, MW ~ 89 000–98 000) were supplied by Sigma-Aldrich. Phosphate-buffered saline (PBS) was acquired as tablets also from Sigma-Aldrich. Sodium citrate tribasic dihydrate (Sigma-Aldrich, ≥99.5%) and citric acid (Sigma-Aldrich, ≥99.5%) were used to prepare citrate buffer with pH 3. Ultrapure water (18.2 MΩ cm) was obtained with a Milli-Q purification system (Merck-Millipore) and used in all preparations. All reagents were used as obtained.

4.2 Instrumentation

A PerkinElmer, model Lambda 35, UV/Vis spectrophotometer was used to record the extinction spectra. Corrected fluorescence emission spectra were recorded with a FluoroLog-3 spectrophotometer (Horiba Jobin Yvon, Tokyo, Japan). Confocal fluorescence microscopy and single-particle spectroscopy measurements were performed on a time-resolved confocal fluorescence microscope, model MicroTime 200, from PicoQuant GmbH (Berlin, Germany). The microscope setup details were previously described.[56] The SymPhoTime software, version 5.3.2.2, from PicoQuant GmbH (Berlin, Germany) was used for data acquisition and analysis. Live cell internalization studies were conducted on a laser scanning confocal microscope, model LSM710, from Zeiss (Jena, Germany). Transmission electron microscopy (TEM) characterization was performed on a Hitachi H-8100 electron microscope operating at 200 kV.

4.3 Tip-selective functionalization of gold nanorods

The tip-selective approach uses the CTAB surfactant bilayer already present in the gold nanorods to direct the dye-labelled oligonucleotides to the tip hot-spots.[33–35] Firstly, the ssDNA sequences indicated above were hybridized in 0.5× PBS for at least 1 h at room temperature using a 25% molar excess of the non-labelled sequence. Then, the functionalization mixture was obtained by adding the dsDNA hybrid (0.5× PBS) to the gold nanorods at a molar ratio of 4000 oligos-per-particle to give a final particle concentration of 1 nM in a volume of 90 μL. The concentration of CTAB was constant at 10 mM during the incubation time. The mixture was allowed to react at room temperature for 1, 3 and 6 hours. At the end of each time interval, the reaction was halted by washing the unbound oligonucleotides in eight centrifugation cycles with resuspension in 500 μL of aqueous CTAB (10 mM). All samples were stored in the suspension at 4 °C until further use. The number of dye-labelled oligonucleotides attached per gold nanorod was determined by a ligand displacement protocol using 2-mercaptoethanol, as reported in ref. 44. For this purpose, a working curve was previously established by measuring the fluorescence intensity from solutions of dye-labelled oligonucleotides with known concentrations in the presence of 2-mercaptoethanol (Fig. S9 of the ESI†). The fluorescence enhancement in the dye-particle nano-assemblies was determined from the emission spectra of each sample before and after dye displacement by ligand exchange with 2-mercaptoethanol. The samples were previously diluted to sub-nanomolar concentrations using either PBST buffer (non-selective functionalization) or aqueous CTAB (tip-selective functionalization). The emission spectra were recorded for excitation wavelengths in the range of 600 to 650 nm in steps of 10 nm. The experimental enhancement factors were calculated from the ratio between the areas of emission spectra of the dye-particle assemblies and that of the same sample after dye displacement (Fig. S10 and Table S3 of the ESI†).

4.4 Non-selective functionalization of gold nanorods

For comparison purposes, a non-selective functionalization approach was used for the attachment of dye-labelled oligonucleotides onto gold nanorods. This approach consists of a two-step ligand exchange process in which CTAB is first replaced by thiolated mPEG-SH molecules and then by dye-labelled dsDNA oligonucleotides following a protocol that was adapted from ref. 42. Briefly, a volume of 2 mL of gold nanorods (0.2 nM) in aqueous CTAB (1 mM) was centrifuged (6000 rpm, 15 min), the supernatant was discarded, and the pellet was resuspended in aqueous mPEG-SH (250 μL, 10 μM) and Tween 20 (250 μL, 0.2 wt%). The solution was centrifuged (6000 rpm, 15 min) and the supernatant was replaced again with mPEG-SH and Tween 20. This procedure was repeated two times to wash away the CTAB detergent. The second ligand exchange begins with hybridization of the ssDNA sequences, as described in the previous section. After that, the hybrid (35 μL) was added to the PEG-stabilized gold nanorods (10 μL) to obtain the following molar ratios of dye-per-particle: 400, 800, 1600 and 4000, while keeping the particle concentration fixed at *ca.* 2 nM. Then, citrate buffer at pH 3 (20 μL, 0.5 M) and PBS (35 μL, 1×) were added, and functionalization was allowed to proceed for 1 h at room temperature. Finally, the unreacted oligonucleotides were washed by six centrifugation cycles with resuspension in PBST buffer (mixture of PBS with Tween 20, 0.01 wt%). The surface charge of tip- and NS-functionalized gold nanorod samples was assessed from measurements of zeta potential (Table S4 of the ESI†).

4.5 Single-particle fluorescence spectroscopy

Fluorescence emission from dye-particle nano-assemblies in colloidal suspension was characterized by Fluorescence Correlation Spectroscopy (FCS). These measurements were performed with picosecond diode laser excitation at 639 nm and by selecting emission with a bandpass filter centred at 695 nm

and a transmission window of 55 nm. The emission intensity time traces were collected from a sub-nanomolar suspension of functionalized gold nanorods (*ca.* 10 μm above the coverslip surface) during a time interval of 60 or 120 s for several excitation powers in the range from 4.4×10^{-3} to 4.4 kW cm^{-2}. The acquisition in time-tagged time-resolved mode also provided fluorescence decays for the same samples. Single-particle emission intensity and one-photon luminescence measurements were characterized on surface-immobilized samples. For this purpose, NS- or tip-functionalized gold nanorods were diluted to a sub-nanomolar concentration in a PVA solution (1% v/v) and deposited on glass coverslips by spin-coating. Fluorescence emission was measured using excitation at 639 nm with a power of 4.4×10^{-2} kW cm^{-2} to minimize photodamage effects, which were evaluated from several consecutive image acquisitions using a scanning resolution of 0.156 nm per pixel and an integration time per pixel of 0.6 ms. Then, the excitation wavelength was changed to 482 nm and an excitation power of *ca.* 50 kW cm^{-2} was used to measure the one-photon luminescence spectrum from individual gold nanorods. The spectral lineshape was fitted with a Lorentzian function using a home-made MATLAB program. The corresponding diffraction-limited spots in the fluorescence images obtained with excitation at 639 nm were fitted with a 2D-Gaussian using an adapted MATLAB routine for point-spread function fitting.

4.6 Model simulations

The method of discrete dipole approximation was used to obtain estimates of the plasmonic enhancement effect of a gold nanorod on the fluorescence emission from Atto-647N dye. A full detailed description of the calculation procedures can be found in ref. 37 and 57. In this work, the simulated particle was a spherically capped cylinder with a diameter of 25 nm and a length of 61 nm. The volume of this particle was discretized as an array of cubic elements with a side of 0.25 nm. The values reported for the dielectric function of gold by Johnson and Christy were renormalized to the dielectric constant of water in order to describe the particle and its surrounding environment.[58] The fluorescent dye was modelled as a point-like dipole emitting at specific wavelengths each representing a spectral component within the dye's emission spectrum.[37] The magnitude of the dye's transition dipole moment was calculated from its rate of spontaneous emission,[59] using the fluorescence quantum yield and lifetime determined for the dye-labelled oligonucleotide in water, ϕ_0 = 0.57 and τ = 4 ns (data not shown). The separation between the emitter and the metal surface was kept constant at a distance of about 4 nm that matches the DNA spacer length. Two conditions were considered regarding the emitter's transition dipole orientation: it was either assumed to be orthogonal to the metal surface or it was orientationally averaged over three independent directions of space. For each probed position, the fluorescence enhancement, $F/F^0|_{calc}$, was estimated from DDA simulations from the product of the excitation rate enhancement, E_{exc}, and the relative emission quantum yield of the dye modified by the plasmonic particle, $F/F^0|_{calc} = E_{exc} \times \phi/\phi^0$. The excitation rate enhancement was obtained from $E_{exc} = |\mathbf{E}|^2/|\mathbf{E}_0|^2$, which is the near-field enhancement at the incident wavelength in the position assumed for the dye molecule. The relative emission quantum yield of the dye, ϕ/ϕ_0, was calculated from the radiative, K_r, and non-radiative, K_{nr}, decay rates modified by the plasmonic antenna using the theoretical formalism described by D'Agostino *et al.*[60]

Conflicts of interest

There are no conflicts to declare.

Acknowledgements

The authors gratefully acknowledge financial support from Fundação para a Ciência e a Tecnologia, FCT through national projects (UID/BIO/04565/2019, UID/QUI/00100/2019 and UID/Multi/04326/2019). DB acknowledges a Ph.D. grant from the BIOTECnico Program (PD/BD/113630/2015). PMRP acknowledges financial support from FCT through grant SFRH/BPD/111906/2015. Hélvio M. R. Simões is acknowledged for providing a sample of gold nanospheres coated with ssDNA oligonucleotides.

Notes and references

1 A. B. Chinen, C. M. Guan, J. R. Ferrer, S. N. Barnaby, T. J. Merkel and C. A. Mirkin, *Chem. Rev.*, 2015, **115**, 10530–10574.
2 S. S. Lucky, K. C. Soo and Y. Zhang, *Chem. Rev.*, 2015, **115**, 1990–2042.
3 P. Biagioni, J.-S. Huang and B. Hecht, *Rep. Prog. Phys.*, 2012, **75**, 024402.
4 H. Chen, L. Shao, Q. Lia and J. Wang, *Chem. Soc. Rev.*, 2013, **42**, 2679–2724.
5 R. Bardhan, N. K. Grady, J. R. Cole, A. Joshi and N. J. Halas, *ACS Nano*, 2009, **3**, 744–752.
6 T. Ming, L. Zhao, Z. Yang, H. Chen, L. Sun, J. Wang and C. Yan, *Nano Lett.*, 2009, **9**, 3896–3903.
7 H. Su, Y. Zhong, T. Ming, J. Wang and K. S. Wong, *J. Phys. Chem. C*, 2012, **116**, 9259–9264.
8 N. S. Abadeer, M. R. Brennan, W. L. Wilson and C. J. Murphy, *ACS Nano*, 2014, **8**, 8392–8406.
9 T. Ming, L. Zhao, H. Chen, K. C. Woo, J. Wang and H.-Q. Lin, *Nano Lett.*, 2011, **11**, 2296–2303.
10 L. Zhao, T. Ming, H. Chen, Y. Liang and J. Wang, *Nanoscale*, 2011, **3**, 3849–3859.
11 L. Zhao, T. Ming, L. Shao, H. Chen and J. Wang, *J. Phys. Chem. C*, 2012, **116**, 8287–8296.
12 B. Jang, J. Y. Park, C. H. Tung, I. H. Kim and Y. Choi, *ACS Nano*, 2011, **5**, 1086–1094.
13 Y. Zhang, J. Qian, D. Wang, Y. Wang and S. He, *Angew. Chem., Int. Ed.*, 2013, **52**, 1148–1151.

14 Q. Jia, J. Ge, W. Liu, S. Liu, G. Niu, L. Guo, H. Zhang and P. Wang, *Nanoscale*, 2016, **8**, 13067–13077.
15 C. Zhang, X. Cheng, M. Chen, J. Sheng, J. Rend, Z. Jiang, J. Cai and Y. Hu, *Colloids Surf., B*, 2017, **160**, 345–354.
16 Y. Huang, Q. Liu, Y. Wang, N. He, R. Zhao, J. Choo and L. Chen, *Nanoscale*, 2019, **11**, 12220–12229.
17 Z. Wang, S. Zong, J. Yang, J. Li and Y. Cui, *Biosens. Bioelectron.*, 2011, **26**, 2883–2889.
18 Q. Wu, L. Chen, L. Huang, J. Wang, J. Liu, C. Hu and H. Han, *Biosens. Bioelectron.*, 2015, **74**, 16–23.
19 H. Jin, X. Liu, R. Gui and Z. Wang, *Colloids Surf., B*, 2015, **128**, 498–505.
20 X.-W. Wang, W. Gao, H. Fan, D. Ding, X.-F. Lai, Y.-X. Zou, L. Chen, Z. Chen and W. Tan, *Nanoscale*, 2016, **8**, 7942–7948.
21 J.-Y. Zeng, M.-K. Zhang, M.-Y. Peng, D. Gong and X.-Z. Zhang, *Adv. Funct. Mater.*, 2018, **28**, 1705451.
22 E. Gournaris, W. Park, S. Cho, D. J. Bentrem, A. C. Larson and D.-H. Kim, *ACS Appl. Mater. Interfaces*, 2019, **11**, 21353–21359.
23 X. Huang, X.-J. Tian, W.-L. Yang, B. Ehrenberg and J.-Y. Chen, *Phys. Chem. Chem. Phys.*, 2013, **15**, 15727–15733.
24 X. Ke, D. Wang, C. Chen, A. Yang, Y. Han, L. Ren, D. Li and H. Wang, *Nanoscale Res. Lett.*, 2014, **9**, 666.
25 T. Zhao, K. Yu, L. Li, T. Zhang, Z. Guan, N. Gao, P. Yuan, S. Li, S. Q. Yao, Q.-H. Xu and G. Q. Xu, *ACS Appl. Mater. Interfaces*, 2014, **6**, 2700–2708.
26 X. Wu, F. Gao, L. Xu, H. Kuang, L. Wang and C. Xu, *RSC Adv.*, 2015, **5**, 97898–97902.
27 L. Qin, X. He, L. Chen and Y. Zhang, *ACS Appl. Mater. Interfaces*, 2015, **7**, 5965–5971.
28 L. Wang, Q. Song, Q. Liu, D. He and J. Ouyang, *Adv. Funct. Mater.*, 2015, **25**, 7017–7027.
29 G. Wei, J. Yu, J. Wang, P. Gu, D. J. S. Birch and Y. Chen, *J. Biomed. Opt.*, 2016, **21**, 097001.
30 D. C. S. Lio, C. Liu, C. Wiraja, B. Qiu, C. W. Fhu, X. Wang and C. Xu, *ACS Sens.*, 2018, **3**, 1647–1655.
31 W. Dai, H. Dong, K. Guo and X. Zhang, *Chem. Sci.*, 2018, **9**, 1753–1759.
32 H. Chen, F. Yuan, S. Wang, J. Xu, Y. Y. Zhang and L. Wang, *Biosens. Bioelectron.*, 2013, **48**, 19–25.
33 K. K. Caswell, J. N. Wilson, U. H. F. Bunz and C. J. Murphy, *J. Am. Chem. Soc.*, 2003, **125**, 13914–13915.
34 S. T. S. Joseph, B. I. Ipe, P. Pramod and K. G. Thomas, *J. Phys. Chem. B*, 2006, **110**, 150–157.
35 Z. Nie, D. Fava, E. Kumacheva, S. Zou, G. C. Walker and M. Rubinstein, *Nat. Mater.*, 2007, **6**, 609–614.
36 Y. Fu, J. Zhang and J. R. Lakowicz, *J. Am. Chem. Soc.*, 2010, **132**, 5540–5541.
37 S. Khatua, P. M. R. Paulo, H. Yuan, A. Gupta, P. Zijlstra and M. Orrit, *ACS Nano*, 2014, **8**, 4440–4449.
38 E. Wientjes, J. Renger, R. Cogdell and N. F. van Hulst, *J. Phys. Chem. Lett.*, 2016, **7**, 1604–1609.
39 W. Zhang, M. Caldarola, X. Lu, B. Pradhan and M. Orrit, *Phys. Chem. Chem. Phys.*, 2018, **20**, 20468–20475.
40 D. P. Szekrényes, S. Pothorszky, D. Zámbó, Z. Osváth and A. Deák, *J. Phys. Chem. C*, 2018, **122**, 1706–1710.
41 B. E. Janicek, J. G. Hinman, J. J. Hinman, S. H. Bae, M. Wu, J. G. Turner, H.-H. Chang, E. Park, R. Lawless, K. S. Suslick, C. J. Murphy and P. Y. Huang, *Nano Lett.*, 2019, **19**, 6308–6314.
42 J. Li, B. Zhu, Z. Zhu, Y. Zhang, X. Yao, S. Tu, R. Liu, S. Jia and C. J. Yang, *Langmuir*, 2015, **31**, 7869–7876.
43 V. Baumann, P. J. F. Röttgermann, F. Haase, K. Szendrei, P. Dey, K. Lyons, R. Wyrwich, M. Gräßel, J. Stehr, L. Ullerich, F. Bürsgensd and J. Rodríguez-Fernández, *RSC Adv.*, 2016, **6**, 103724.
44 L. M. Demers, C. A. Mirkin, R. C. Mucic, R. A. Reynolds, R. L. Letsinger, R. Elghanian and G. Viswanadham, *Anal. Chem.*, 2000, **72**, 5535–5541.
45 H. D. Hill, J. E. Millstone, M. J. Banholzer and C. A. Mirkin, *ACS Nano*, 2009, **3**, 418–424.
46 G. Wang, Y. Akiyama, T. Takarada and M. Maeda, *Chem. – Eur. J.*, 2016, **22**, 258–263.
47 G. Wang, Y. Akiyama, N. Kanayama, T. Takarada and M. Maeda, *Small*, 2017, **13**, 1702137.
48 N. J. Hestand and F. C. Spano, *Chem. Rev.*, 2018, **118**, 7069–7163.
49 M. P. Busson, B. Rolly, B. Stout, N. Bonod, J. Wenger and S. Bidault, *Angew. Chem., Int. Ed.*, 2012, **51**, 11083–11087.
50 A. Ortega and J. García de la Torre, *J. Chem. Phys.*, 2003, **119**, 9914–9919.
51 N. D. Burrows, W. Lin, J. G. Hinman, J. M. Dennison, A. M. Vartanian, N. S. Abadeer, E. M. Grzincic, L. M. Jacob, J. Li and C. J. Murphy, *Langmuir*, 2016, **32**, 9905–9921.
52 K. L. Blythe and K. A. Willets, *J. Phys. Chem. C*, 2016, **120**, 803–815.
53 T. Liu, S. Liu, W. Jiang and W. Wang, *ACS Nano*, 2019, **13**, 6279–6286.
54 E. Tavares, J. A. Macedo, P. M. R. Paulo, C. Tavares, C. Lopes and E. P. Melo, *Biochim. Biophys. Acta*, 2014, **1842**, 981–991.
55 D. Punj, R. Regmi, A. Devilez, R. Plauchu, S. B. Moparthi, B. Stout, N. Bonod, H. Rigneault and J. Wenger, *ACS Photonics*, 2015, **2**, 1099–1107.
56 P. M. R. Paulo, D. Botequim, A. Jóskowiak, S. Martins, D. M. F. Prazeres, P. Zijlstra and S. M. B. Costa, *J. Phys. Chem. C*, 2018, **122**, 10971–10980.
57 R. Teixeira, P. M. R. Paulo and S. M. B. Costa, *J. Phys. Chem. C*, 2015, **119**, 21612–21619.
58 P. B. Johnson and R. W. Christy, *Phys. Rev. B: Solid State*, 1972, **6**, 4370–4380.
59 L. Novotny and B. Hecht, *Principles of Nano-Optics*, Cambridge University Press, Cambridge, 2012.
60 S. D'Agostino, F. Della Sala and L. C. Andreani, *Phys. Rev. B: Condens. Matter Mater. Phys.*, 2013, **87**, 205413.